Journal of the European Ceramic Society 39 (2019) 2680–2684

Contents lists available at ScienceDirect

Journal of the European Ceramic Society

journal homepage: www.elsevier.com/locate/jeurceramsoc

Original Article

Two novel low permittivity microwave dielectric ceramics Li_2TiMO_5 (M = Ge, Si) with abnormally positive τ_f

Kai Cheng[a,b], Ying Tang[b,*], Huaicheng Xiang[b], Chunchun Li[b,c], Liang Fang[a,b,*], Yihua Sun[a,*]

[a] Key Laboratory of Inorganic Nonmetallic Crystalline and Energy Conversion Materials, College of Materials and Chemical Engineering, China Three Gorges University, Yichang, 443002, China

[b] Guangxi Key Laboratory of Optical and Electronic Materials and Devices. College of Material Science and Engineering, Guilin University of Technology, Guilin, 541004, China

[c] College of Information Science and Engineering, Guilin University of Technology, Guilin, 541004, China

ARTICLE INFO

Keywords:
Ceramics
Natisite structure
Dielectric properties
Radio and microwave frequency region

ABSTRACT

Two tetragonal natisite structured Li_2TiMO_5 (M = Ge, Si) ceramics fabricated using the conventional solid-state reaction method were investigated in terms of the thermal stability, sintering behavior and dielectric properties at radio (RF) and microwave frequency region. At the optimum sintering temperature of 1140 °C, Li_2TiGeO_5 (LTG) has ε_r ~ 9.43, $Q \times f$ ~ 65,300 GHz (at 14.7 GHz), and τ_f ~ +24.1 ppm/°C, while Li_2TiSiO_5 (LTS) sintered at 1180 °C exhibits ε_r ~ 9.89, $Q \times f$ ~ 38,100 GHz (at 14.2 GHz), and τ_f ~ +50.1 ppm/°C. The positive τ_f values of the present LTG and LTS are abnormal and extremely important for low-ε_r microwave dielectric ceramics, which could behave as a promising τ_f compensator. Moreover, the dielectric spectra of both ceramics revealed a phase transition at low-temperature, exhibiting a dielectric peak, which could account for the negative τ_ε and positive τ_f in operating temperature ranges.

1. Introduction

For broadcasting at high frequencies from radio (RF) to microwave and to millimeter wave ranges, low-loss dielectric materials with a low permittivity (ε_r, shorten the propagation delay time and improve the transmission rate) and near-zero temperature coefficient of resonant frequency ($\tau_f \approx 0$ ppm/°C) are extensively required and studied [1,2]. To satisfy the needs of fast-growing modern communication, much efforts have been made to develop novel dielectric ceramic materials with high performances.

Some silicates have been reported to possess low ε_r below 10, which could be attributed to the low ionic polarizability of Si^{4+} (0.87 Å^3) [3] and the strong effects of the covalent bond of Si-O because of its coordination condition to form [SiO_4] tetrahedron [4]. Previous work on silicate systems mainly focused on cordierite $Mg_2Al_4Si_5O_{18}$, Sr_2AlSiO_7, sillimanite (Al_2SiO_5), $MgSiO_3$, willemite (Zn_2SiO_4), and forsterite Mg_2SiO_4 ceramic materials with low-ε_r (4.73–9.5) and ultra-low dielectric loss (78,500-270,000 GHz) [5–10], which have been proposed to be promising substrate ceramic materials. Although these silicates exhibit high $Q \times f$ values were reported, their high sintering temperature (> 1300 °C) mainly related to chemical refractory of SiO_2 and large negative τ_f values (< -20 ppm/°C) preclude their practical applications to some extent. Considering the same valence and coordination preference of Ge^{4+} and Si^{4+}, it is reasonably expected that germanates would exhibit similar dielectric properties as silicates with the same crystallographic structure. In addition, the sintering temperature of Ge-based ceramics, such as $CaGeO_3$ [11] Zn_2GeO_4 [12], $(Zn_{1-x}Mg_x)_{1.918}GeO_{3.918}$ ($0.2 \le x \le 0.6$) [13] and $Ba_2MGe_2O_7$ (M = Mg and Zn) [14] systems, is much lower than their silicate counterparts. Regarding to these initial progresses of silicate and germanates dielectrics, there still remain broad spaces to explore novel microwave dielectric ceramics.

The natisite-type compounds have a general formula A_2BMO_5 (A = Li^+, Na^+; B = Ti^{4+}, V^{4+}; M = Si^{4+}, Ge^{4+}), in which A, B and M atoms have 6, 5 and 4 nearest oxygen neighbours occupying the wykcoff sites of 4e, 2c, and 2a, respectively. They crystallize in layered structure, consisting of $[BO_5]^{6-}$ square pyramids and $[MO_4]^{4-}$ tetrahedra sharing corner along the b-axis to form a layered band, in which A ions are located between layers [15]. Due to the strong anisotropy of natisite-like structures, previous work mainly focused on the physical properties, such as ionic conductivity and luminous characteristics, as well as the paraelastic-ferroelastic transition of the polycrystalline and

* Corresponding authors at: Key Llaboratory of Inorganic Nonmetallic Crystalline and Energy Conversion Materials, College of Materials and Chemical Engineering, China Three Gorges University, Yichang, 443002, China.

E-mail addresses: tangyinggl001@aliyun.com (Y. Tang), fangliangl001@aliyun.com (L. Fang), sunyihua316181@163.com (Y. Sun).

https://doi.org/10.1016/j.jeurceramsoc.2019.03.017
Received 4 January 2019; Received in revised form 3 March 2019; Accepted 7 March 2019
Available online 08 March 2019
0955-2219/

doped single crystal [16,17]. Considering the potential dielectric performance and structural adjustability of silicates and germanates, two natisite-type Li_2TiMO_5 (M = Si, Ge) ceramics were prepared, and their thermal stability, sintering behavior and dielectric properties at RF and microwave frequency region were then investigated.

2. Experimental procedure

Using conventional solid-state method, Li_2TiGeO_5 (LTG) and Li_2TiSiO_5 (LTS) ceramics were prepared from high purity (> 99.99%) reagents (i.e. Li_2CO_3, TiO_2, SiO_2, and GeO_2). After 6 h of ball milling and 120 °C of drying, the raw materials were calcined for 6 h at 1050 °C. After that, the samples were re-ground and 5 wt% PVA was added as the binder to press into cylindrical disks with the diameter of 10 mm and the height of 5 mm, as well as some discs of 10 mm in diameter and 2 mm in thickness for RF dielectric characteristic under uniaxially pressure of 300 MPa. The green compacts were firstly fired at 550 °C in air for 2 h to expel the organic binder and then sintered from 1080 °C to 1200 °C for 6 h with a heating rate of 5 °C/min.

The phase formation and structure stability were examined by means of thermogravimetry (TG) and differential thermal analysis (DTA) using an analyzer with the simultaneous recording of weight losses and temperature variations under atmosphere using a thermo-analyzer system (DELTA-7, PE). The phase purity of the samples was determined by X-ray powder diffraction (XRD, Cu*Kα*1, X'pert PRO, PANalytical, Netherlands) in the range of 10-120°. The microstructure of the sintered samples was observed by scanning electron microscopy (SEM, JSM6380-LV, Japan). The bulk densities of the sintered samples were measured by the Archimedes' method. The microwave dielectric properties were measured using a network analyzer (N5230A, Agilent Co., Canada) and a temperature chamber (Delta 9039, Delta Design, CA). The temperature coefficient of resonant frequency was measured in the temperature range from 25 °C (T_1) to 85 °C (T_2). The values were calculated as follows:

$$\tau_f(ppm/^oC) = \frac{f_2 - f_1}{f_1(T_2 - T_1)} \times 10^6 \tag{1}$$

where, f_1 and f_2 represent resonant frequencies at temperatures T_1 and T_2, respectively.

In order to analyze the electrical properties of the samples, both sides of optimized discs were polished and fired silver electrode to form parallel plate capacitors. An impedance analyzer (Agilent 4294A) were used to measure the temperature-dependent dielectric characteristics over the frequency range 1kHz-1 MHz at temperature range of -175-120 °C and 300–600 °C, respectively. The linear coefficient of thermal expansion (CTE) was estimated utilizing a thermal dilatometer (DIL402C, NETZSCH, Germany).

3. Results and discussion

In order to understand the formation of both compounds, XRD analyses were carried out on samples sintered at various temperatures for 6 h. As shown in Fig.1, when sintering at 950 °C, it is clear that LTG ceramics exhibit mixed phases, including the main phase LTG and the small amount of TiO_2 and Li_2GeO_3 phases. A similar phenomenon was also observed in LTS, with the secondary phases being SiO_2 and Li_2TiO_3. With increasing the calcination temperature, the amount of secondary phase decreased. As sintering temperatures are above 1050 °C, no additional reflections other than LTG (JCPDS#75-5086) or LTS (JCPDS#82-1955) are detected. In the combination of the results of TG-DSC analysis (more details see in supplementary information Fig. S1), therefore, it reveals that the stable LTG and LTS pure phase can be formed at a high temperature above 1050 °C.

Fig. 2 shows the results of Rietveld refinement and crystal structure for LTG and LTS adopting P/4nmm space group (more refinement data

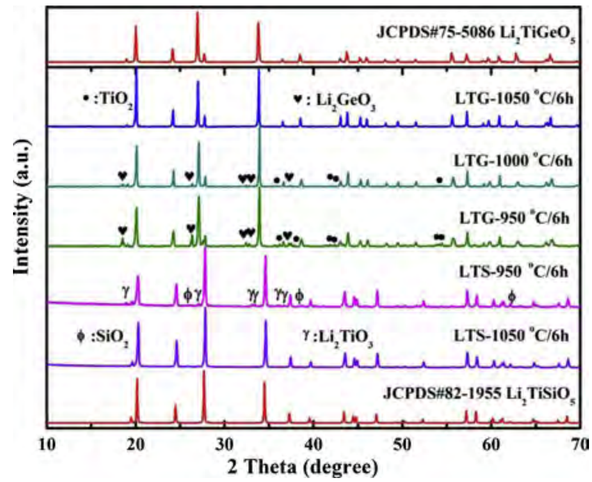

Fig. 1. XRD patterns for LTG and LTS sintered at various temperature.

see in supplementary information Table S1). It demonstrates that Li atoms locate in oxygen octahedral sites while Ge/Si exists in fourfold coordination for both compounds. The crystal structure is built of a layered band of the [TiO_5] square pyramid and [Ge/SiO_4] tetrahedron along the b-axis sharing corners, where Li atoms are located between the layers. In other word, it could be described as the edge-shared [LiO_6] interlaminar octahedra formed polyhedron plane along the b-axis and alternately shared its O1 corner with [Ge/SiO_4] tetrahedron to form a three-dimensional network. As listed in Table1, the unit cell volume and lattice constants of LTS are much smaller than those of LTG, which is mainly ascribed to the differences in M-O(1) bond length, which leads to the change of the structural characteristics of the octahedron. It should be noted that [LiO_6] octahedron are relatively distorted with four short Li-O(1) bonds (λ_1) and two long Li-O(2) bonds (λ_2). The λ_1 of LTG is 2.04861(1) Å, which is similar to that of LTS ˜ 2.0644(1). However, the λ_2 of LTG (2.54491(4) Å) is larger than that of LTS (2.4404(0) Å). For the quantitative evaluation of the crystal structural characteristics, the average octahedral distortion (Δ) of the Li-site was calculated using the following equation [18]:

$$\Delta = \frac{1}{6}\sum\left\{\frac{R_i - R_{av}}{R_{av}}\right\}^2 \tag{2}$$

where R_{av} is the average bond length and R_i is an individual bond length in the oxygen octahedron. The distortion of [LiO_6] octahedron in LTG (11.2×10^{-3}) is more evident than that of LTS (6.6×10^{-3}) due to the different Li-O bond length and O-Li-O bond angles.

The variation of relative densities of both ceramics with the sintering temperature was shown in Fig. 3. As the sintering temperature increased, the relative densities of LTG initially increased and then started to decrease after reached a maximum value with relative densities ˜ 97.5% (theoretical density ρ_{th} = 3.67 g/cm^3) at 1140 °C, while ˜96.4% and ρ_{th} = 3.09 g/cm^3 for LTS specimens sintered at 1180 °C, respectively. The SEM images of the LTG ceramic sintered at 1080 °C–1160 °C for 6 h are shown in Fig. 4. As observed, a relatively porous micro-structure consisting of small grains was observed in the 1080 °C-sintered ceramic. With increasing sintering temperature, the number of pores decreased accompanied by an obvious grain growth. Densification occurred when sintered at 1140 °C, characterized by a dense microstructure with distinct grain boundaries and homogeneous grains. However, when the temperature increased to 1160 °C, large grains (˜ 10 μm) appeared. Microstructural evolution as a function of sintering temperature in LTS was similar to LTG and a dense and uniform microstructure was developed in the sample sintered at 1180 °C for 6 h, as shown in Fig. 4(f–j).

Fig. 5 presents microwave dielectric properties (ε_r, $Q\times f$, and τ_f) dependence on sintering temperature of LTG and LTS ceramics. With

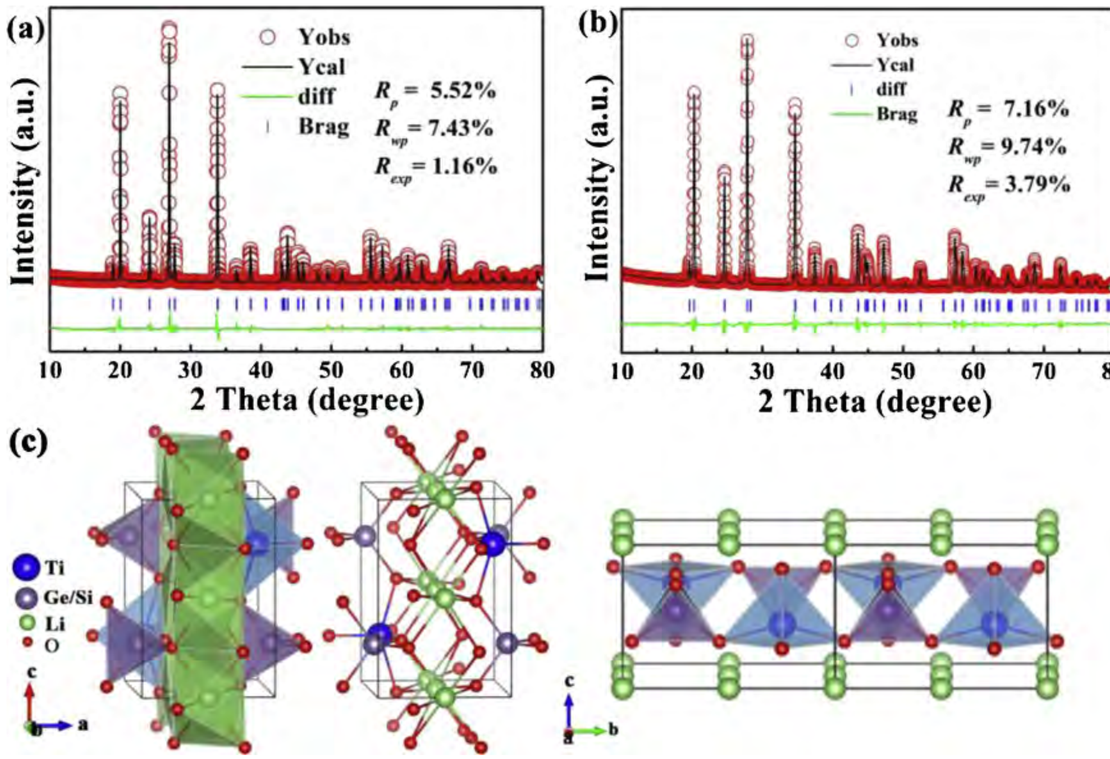

Fig. 2. XRD patterns Rietveld refinement of (a) LTG and (b) LTS samples sintered at 1140 °C and 1180 °C for 6 h, and (c) their crystal structure.

the increase of sintering temperature, both ε_r and $Q \times f$ values increase to the maximum and then decrease, showing a similar trend to the density change, in Fig. 3. Over the sintering temperature range, the saturation values, ε_r ~ 9.43 and $Q \times f$ ~ 65,300 GHz (at 14.7 GHz) for LTG while ε_r ~ 9.89 and $Q \times f$ ~ 38,200 GHz (at 14.2 GHz) were obtained for LTS sintered at their optimum sintering temperature. It was noted that LTG exhibits lower ε_r and higher $Q \times f$ values in comparison to LTS. In regard to the factors effecting the microwave dielectric properties, there are in general two components: the intrinsic factors and the extrinsic factors. The extrinsic factors, including impurities, grain boundaries, grain morphology and shape, secondary phase, pores, etc., almost could be neglected in the present optimum specimens due to the dense and homogeneous microstructure and no secondary phase. Meanwhile, the intrinsic factors are closely related to the crystal structure, which might be analyzed by means of the related characteristic parameter as ionic polarizability of the primitive cell, the packing fraction. The fundamental contribution for dielectric permittivity can be reflected by the Clausius-Mosotti equation, by which the theoretical dielectric permittivity $\varepsilon_{r\text{-calculated}}$ value can be calculated and Shannon additive rule [19] as follows:

$$\varepsilon_r = \frac{3}{1 - b\alpha_D^T/Vm} - 2 \tag{3}$$

where α_D^T is the molecular polarizability of all the constituent ions, V_m the cell volume, and b represents a constant value, $(4\pi/3)$. Accordingly, the theoretical permittivity of LTG and LTS is calculated to be 8.93 and 9.69 respectively, slightly deviating from the measured ε_r, indicating that the solely ionic polarization mechanism contributes to the dielectric response in the microwave frequency band. Therefore, the ε_r difference can be interpreted by the lower α_D^T/V_m value of LTG ~ 0.1745 than that of LTS ~ 0.1776 [20].

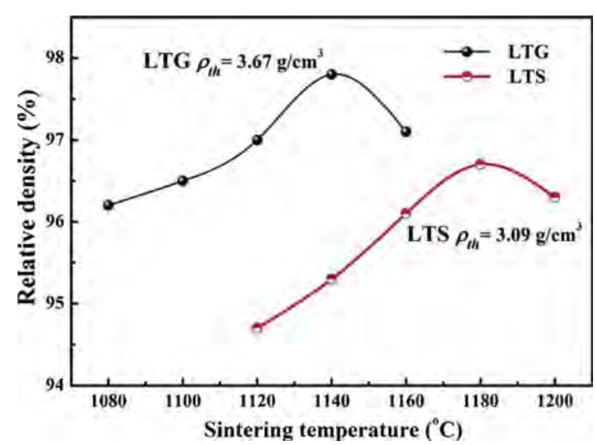

Fig. 3. The variation of relative density of both samples sintered at various temperature.

Kim et al. [21] reported that the $Q \times f$ values were closely related to the packing fraction as defined by summing the volume of packed ions (V_{PI}) over the volume of a primitive unit cell (V_{PUC}), expressed as follows:

$$f\,(\%) = \frac{Z \times V_{PI}}{V_{PUC}} \times 100 \tag{4}$$

where Z is the number of formula units per unit cell. The calculated

Table 1
Crystallographic data obtained from Rietveld refinement and average octahedral distortion (Δ) for Li_2TiMO_5 (M = Ge, Si) specimens.

composition	$a=b$ (Å)	c (Å)	V	R_{wp} (%)	R_p (%)	R_{exp} (%)	Δ ($\times 10^{-3}$)
Li_2TiGeO_5	6.44402(1)	4.43996(0)	194.01	5.52	7.43	1.16	11.2 ± 0.2
Li_2TiSiO_5	6.14003(0)	4.43560(5)	182.38	7.16	9.74	3.79	6.6 ± 0.1

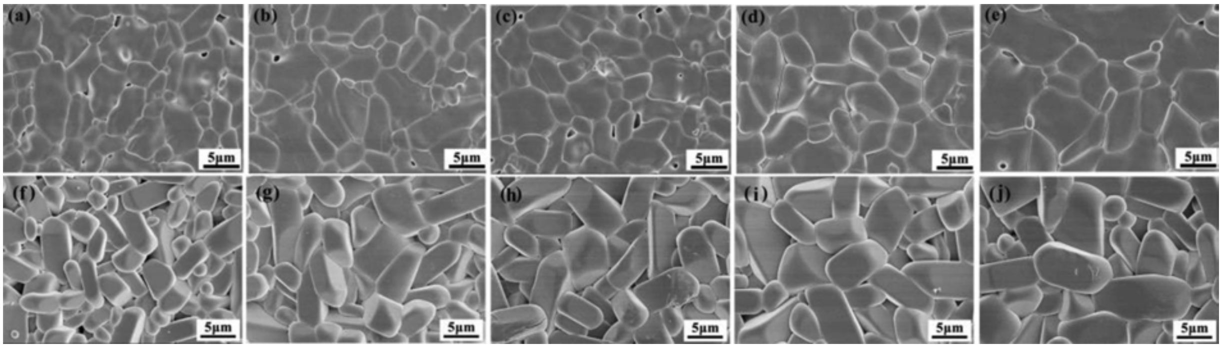

Fig. 4. The temperature dependence of SEM images of the polished and thermally etched surface of (a–e) LTG and (f–j) LTS sintered at various temperatures, respectively.

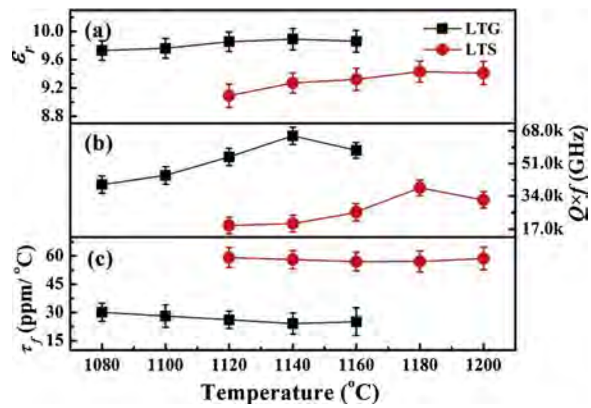

Fig. 5. The variation of microwave dielectric properties (ε_r, $Q\times f$, and τ_f) of Li_2TiMO_5 (M = Ge, Si) ceramics as a function of sintering temperature.

packing fraction of LTG is 52.20%, which is higher than that of LTS (˜49.52%), thus, leading to the resultant higher $Q \times f$ value of LTG compared to LTS, which means that the variation of $Q \times f$ values for both samples could be well evaluated by the packing fraction.

Temperature stability of dielectric properties of ceramic is another significant concern for practical application. The measured temperature coefficients of resonance frequency of LTG and LTS fluctuated at +24.1 ppm/°C and +50.1 ppm/°C, respectively. Generally, the ε_r of the dielectric ceramics is proportional to the τ_f, that is, the low ε_r corresponds to the low τ_f [22]. Ceramics usually have negative τ_f values when ε_r is less than 10, as summarized in Table 2. The positive τ_f values of the present LTG and LTS are rare and extremely important to be utilized as τ_f compensator to adjust the negativeτ_f values of the other low-ε_r materials. Additionally, it is worth noting that the sintering temperature of LTG and LTS are much lower than others. Now the question arises why these two LTG and LTS have positive τ_f values and what is the reason for their difference inτ_f values. According to the ε_r-τ_f relationship [23], the τ_f value was affected by the temperature coefficient of relative permittivity (τ_ε) and the linear thermal expansion coefficient (α_L), as in Eq. (5):

$$\tau_f = -\left(\frac{\tau_\varepsilon}{2} + \alpha_L\right) \tag{5}$$

To further understand the close relationship between τ_f and τ_ε, Fig. 6(a–b) illustrate the temperature dependence of ε_r and *tanδ* of optimized LTG and LTS ceramics at two selected various frequencies (100 kHz and 1 MHz) over the temperature scanning range of -150 to 120 °C. According to Fig. 6(a), with the increase in temperature, the dielectric constant for both frequencies (100 kHz and 1 MHz) of the LTG ceramic sample continued to increase before -51.5 °C, followed by a gentle decline trend up to 120 °C. Theτ_ε value calculated to be -70 ppm/°C at -51.5 to 120 °C, which is attributed to a second order phase transition into the nonpolar phase. Previous studies of electrical, thermal, optical and elastic properties had also confirmed this phase transition [16,17]. However, as shown in Fig. 6(b), only a downward trend was observed in LTS ceramics, where the τ_ε value was -135 ppm/°C, which probably due to the corresponding phase transition occurred at lower temperature beyond the measuring temperature range (-150 °C-120 °C). It should be investigated in the future. Fig. 7 shows the linear thermal expansion coefficient (CTE) curves of optimized LTG and LTS ceramics. The insert of Fig. 7 gives the change of CTE with different temperatures, and the average CTE of LTG is 10.10 ppm/°C and 11.70 ppm/°C for LTS. Using Eq. 5, the LTG and LTS also have negative τ_ε values (−68.4 ppm/°C and −123.6 ppm/°C), which corresponds to the test results in Fig. 6. To sum up, in this work, the abnormally positive τ_f values of low ε_r microwave dielectric ceramics Li_2TiMO_5 (M = Ge, Si) are caused by the phase transition mechanism in low temperature.

Table 2
Comparison of microwave dielectric properties of Li_2TiMO_5 (M = Ge, Si) ceramics versus other low-ε_r (< 10) Si-/Ge- containing systems.

composition	ε_r	$Q \times f$ (GHz)	τ_f (ppm/°C)	T_s (°C)	Ref.
Al_2SiO_5	4.73	41,800	−17.0	1525	[7]
$Mg_2Al_4Si_5O_{18}$	6.20	39,000	−39.2	1450	[5]
$BaAl_2Si_2O_8$	6.40	44,800	−46.9	1475	[2]
Zn_2SiO_4	6.60	198,400	−41.6	1325	[9]
$MgSiO_3$	6.70	16,000	−17.0	1380	[8]
$CaSiO_3$	6.8	27,000	−11.0	1300	[11]
Zn_2GeO_4	6.90	102,700	−32.4	1300	[12]
$Sr_2Al_2SiO_7$	7.2	33,000	−37.0	1525	[6]
Mg_2SiO_4	7.50	240,000	−63.0	1450	[10]
Li_2TiGeO_5	9.43	65,344	+24.1	1140	This work
Li_2TiSiO_5	9.89	38,516	+50.1	1180	This work

4. Conclusion

Tetragonal natisite structure ceramics Li_2TiMO_5 (M = Si, Ge) were synthesized at 1050–1200 °C using a conventional solid-state method. The dielectric properties were characterized over a broad frequency (RF-microwave) and temperature range (-150-120 °C). The densification sintering temperature of the LTG ceramic ˜ 1140 °C is lower than that of LTS ˜ 1180 °C. In addition, both low-ε_r ceramic LTG (ε_r ˜ 9.43) and LTS (ε_r ˜ 9.89) exhibited abnormally positive τ_f valuesτ_f ˜ +24.1 and τ_f ˜ +50.1 ppm/°C, respectively, which were proved to be induced by the distinctly dielectric peak that was associated with phase transition in low temperature. Within the measured at RF range, the impedance spectra of LTG and LTS can be analyzed using two equivalent circuit elements, one related to grain resistance and the other to grain boundary resistance.

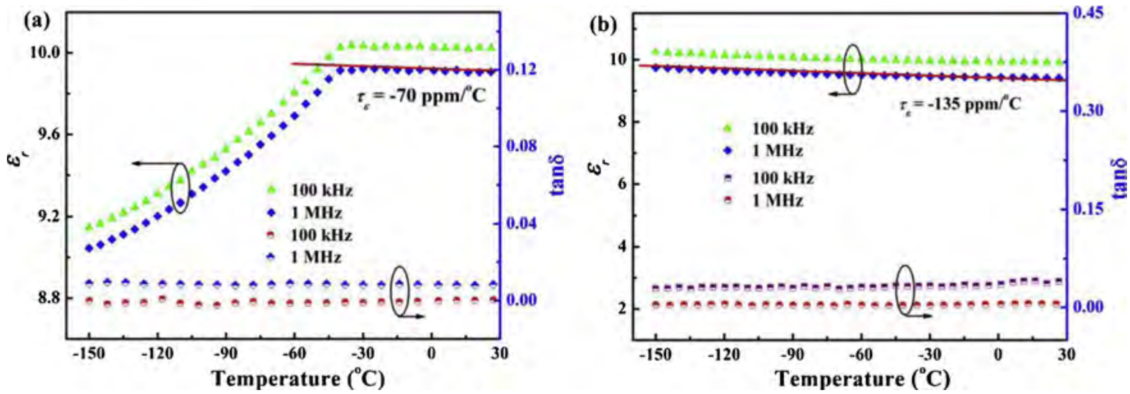

Fig. 6. Temperature and frequency dependences of dielectric constant and dielectric loss for (a, c) LTG specimen and (b, d) LTS specimen.

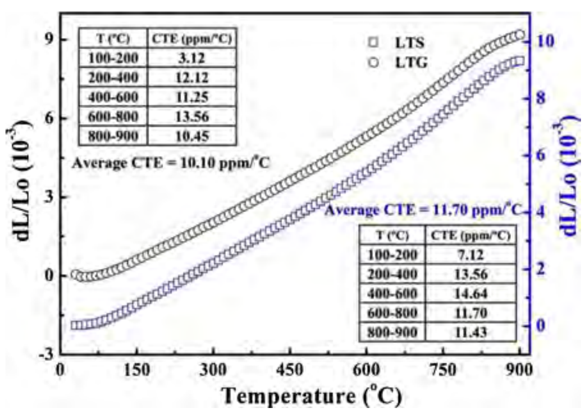

Fig. 7. The thermal expansion curves of LTG and LTS at a temperature range of.25–900 °C.

Acknowledgments

This work was supported by Natural Science Foundation of China (Nos. 21761008 and 21561008), the Natural Science Foundation of Guangxi Zhuang Autonomous Region (Nos. 2018GXNSFAA138175, 2015GXNSFFA139003 and 2018GXNSFAA281093), and Projects of Department of Science and Technology of Guangxi (Nos. AA18118008 and AA18118034) and Guilin (No. 20170225), Projects of Department of Education of Guangxi (No. 2018Ky0255). Author Y. Sun gratefully acknowledges the State Scholarship fund of the China Scholarship Council (No. CSC201708420285).

Appendix A. Supplementary data

Supplementary material related to this article can be found, in the online version, at doi:https://doi.org/10.1016/j.jeurceramsoc.2019.03.017.

References

[1] M.T. Sebastian, H. Jantunen, Low loss dielectric materials for LTCC applications: a review, Int. Mate. Rev. 53 (2008) 57–90.
[2] W. Lei, Z.Y. Zou, Z.H. Chen, B. Ullah, A. Zeb, X.K. Lan, Controllable τ_f value of barium silicate microwave dielectric ceramics with different Ba/Si ratios, J. Am. Ceram. Soc. 101 (2018) 25–30.
[3] K. Cheng, C.C. Li, H.C. Xiang, Y.H. Sun, L. Fang, $LiYGeO_4$: novel low permittivity microwave dielectric ceramics with intrinsic low sintering temperature, Mater. Lett. 228 (2018) 96–99.
[4] R.D. Shannon, Dielectric polarizabilities of ions in oxides and fluorides, J. Appl. Phys. 73 (1993) 348–366.
[5] Z.Y. Zou, X.K. Lan, W.Z. Lu, G.F. Fan, X.H. Wang, X.C. Wang, P. Fu, W. Lei, Novel high curie temperature $Ba_2ZnSi_2O_7$ ferroelectrics with low-permittivity microwave dielectric properties, Ceram. Int. 42 (2016) 16387–16391.
[6] K.X. Song, P. Liu, H.X. Lin, W.T. Su, J. Jiang, S. Wu, J. Wu, Z.H. Ying, H.B. Qin, Symmetry of hexagonal ring and microwave dielectric properties of $(Mg_{1-x}Ln_x)_2Al_4Si_5O_{18+x}$ (Ln = La, Sm) cordierite-type ceramics, J. Eur. Ceram. Soc. 36 (2016) 1167–1175.
[7] K.M. Manu, T. Joseph, M.T. Sebastian, Temperature compensated $Sr_2Al_2SiO_7$ ceramic for microwave applications, J. Mater. Chem. Phys. 133 (2012) 21–23.
[8] I.J. Induja, M.T. Sebastian, Microwave dielectric properties of mineral sillimanite obtained by conventional and cold sintering process, J. Eur. Ceram. Soc. 37 (2017) 2143–2147.
[9] M.E. Song, J.S. Kim, M.R. Joung, S. Nahm, Y.S. Kim, J.H. Paik, Synthesis and microwave dielectric properties of $MgSiO_3$ ceramics, J. Am. Ceram. Soc. 91 (2008) 2747–2750.
[10] Y.P. Guo, H. Ohsato, K. Kakimoto, Characterization and dielectric behavior of willemite and TiO_2-doped willemite ceramics at millimeter-wave frequency, J. Eur. Ceram. Soc. 26 (2006) 1827–1830.
[11] S.Q. Meng, Z.X. Yue, H. Zhuang, F. Zhao, L.T. Li, Microwave dielectric properties of $Ba_3(VO_4)_2$-Mg_2SiO_4, composite ceramics, J. Am. Ceram. Soc. 93 (2010) 359–361.
[12] M. Valant, D. Suvorov, Glass-free low-temperature cofired ceramics: calcium germanates, silicates and tellurates, J. Eur. Ceram. Soc. 24 (2004) 1715–1719.
[13] X.H. Ma, S.H. Kweon, M. Im, S. Nahm, Low-temperature sintering and microwave dielectric properties of B_2O_3-added ZnO-deficient Zn_2GeO_4 ceramics for advanced substrate application, J. Eur. Ceram. Soc. 38 (2018) 4682–4688.
[14] Y.J. Eoh, E.S. Kim, High quality factor of $(Zn_{0.6}Mg_{0.4})_{1.918}GeO_{3.918}$ microwave dielectrics, Ceram. Int. 41 (2015) S537–S543.
[15] C.C. Li, C.Z. Yin, J.Q. Chen, H.C. Xiang, Y. Tang, L. Fang, Crystal structure and dielectric properties of germanate melilites $Ba_2MGe_2O_7$ (M = Mg and Zn) with low permittivity, J. Eur. Ceram. Soc. 38 (2018) 5246–5251.
[16] A. Sieradzki, A. Pietraszko, R. Poprawski, Crystal structure and pressure effect of ferroelastic phase transition in Li_2TiGeO_5 crystal, Integr. Ferroelectr. 62 (2004) 79–82.
[17] A. Ziadi, G. Thiele, B. Elouadi, The crystal structure of Li_2TiSiO_5, J. Solid State Chem. 109 (1994) 112–115.
[18] T. Hirata, Oxygen Position, octahedral distortion, and bond-valence parameter from bond lengths in $Ti_{1-x}Sn_xO_2$ (0 < x < 1), J. Am. Ceram. Soc. 83 (2000) 3205–3207.
[19] A.J. Bosman, E.E. Havinga, Temperature dependence of dielectric constants of cubic ionic compounds, Phys. Rev. Lett. 129 (1963) 1593–1600.
[20] L.X. Pang, D. Zhou, D.W. Wang, J.X. Zhao, W.G. Liu, Z.X. Yue, I.M. Reaney, Temperature stable $K_{0.5}(Nd_{1-x}Bi_x)_{0.5}MoO_4$ microwave dielectrics ceramics with ultra-low sintering temperature, J. Am. Ceram. Soc. 101 (2018) 1806–1810.
[21] E.S. Kim, B.S. Chun, R. Freer, R.J. Cernik, Effects of packing fraction and bond valence on microwave dielectric properties of $A^{2+}B^{6+}O_4$ (A^{2+}: Ca, Pb, Ba; B^{6+}: Mo, W) ceramics, J. Eur. Ceram. Soc. 30 (2010) 1731–1736.
[22] W.J. Luo, L.X. Li, S.H. Yu, Z. Sun, B.W. Zhang, F. Xia, Structural, Raman spectroscopic and microwave dielectric studies on high-Q materials in Ge-doped $ZnTiNb_2O_8$ systems, J. Alloys. Compd. 741 (2018) 969–974.
[23] C.H. Su, F.C. Lin, T.M. Chu, C.L. Huang, Structural characteristics and microwave dielectric properties of low-firing $Ba(Co_{1-x}Mg_x)_2(VO_4)_2$ (x = 0-1) ceramics, J. Alloys. Compd. 686 (2016) 608–615.